

Low-energy pion production with 800 MeV/N ^{20}Ne

J. Chiba and K. Nakai

Department of Physics, University of Tokyo, Tokyo, Japan
and Lawrence Berkeley Laboratory, University of California, Berkeley, California 94720

I. Tanihata

Laboratory for Nuclear Studies, Osaka University, Osaka, Japan
and Lawrence Berkeley Laboratory, University of California, Berkeley, California 94720

S. Nagamiya, H. Bowman, J. Ingersoll, and J. O. Rasmussen

Lawrence Berkeley Laboratory, University of California, Berkeley, California 94720

(Received 2 February 1979)

Doubly differential cross sections for production of positive pions ($20 \text{ MeV} \leq T_{\pi}^{\text{Lab}} \leq 100 \text{ MeV}$) in bombardment of ^{20}Ne on NaF, Cu and Pb targets at 800 MeV/N have been measured with a range telescope. The results showed that the angular distribution of low-energy pions in the nucleon-nucleon center of mass ($T_{\pi}^{\text{c.m.}} \leq 50 \text{ MeV}$) was isotropic, even 90° peaking at $\sim 15 \text{ MeV c.m.}$ The intermediate-energy pions ($50 \leq T_{\pi}^{\text{c.m.}} \leq 300 \text{ MeV}$) were forward and backward peaked, reflecting the individual nucleon-nucleon process in the isobar model of production. The observed cross sections were shown to be generally reproduced by an incoherent superposition of the experimental ($p + \text{nucleus}$) cross sections.

[NUCLEAR REACTIONS NaF, Cu, Pb(^{20}Ne , π^+)X, $E/A = 800 \text{ MeV/nucleon}$; measured $\sigma(E_{\pi}, \theta_{\pi})$, $E_{\pi} = 20\text{--}100 \text{ MeV}$, $\theta_{\pi} = 30\text{--}150^\circ$.]

I. INTRODUCTION

The study of pion production in nucleus-nucleus collisions provides unique and interesting information on the reaction mechanism as well as pion interactions in nuclei.

There have been several experimental studies of pion production in nucleus-nucleus collisions. Except for the earlier work by Baldin *et al.*¹ and Schimmerling *et al.*,² most of the work was done at the Berkeley BEVALAC. Papp *et al.*³ studied high-energy pions produced at forward angles by light projectiles, and showed that the pion momentum spectra could be explained by an individual nucleon-nucleus collision model, taking into account the Fermi motion of nucleons in projectiles. Jakobsson *et al.*⁴ were also able to explain their data on pion multiplicity distributions with the individual nucleon-nucleon collision model. On the other hand, the pion multiplicity data with the streamer chamber taken by Poe *et al.*⁵ were explained with the fireball model by Gyulassy *et al.*⁶ Certainly more experimental studies are required to distinguish between the models. It is also of interest to look for any phenomena which are not explained by those models.

In the present work, we studied the low-energy pion production in high-energy nucleus-nucleus collisions. We started this study (for $20 \leq T_{\pi}^{\text{Lab}} \leq 100 \text{ MeV}$) in parallel with the work by Nagamiya *et al.*,⁷ where high-energy pions were measured ($50 \leq T_{\pi}^{\text{Lab}} \leq 1000 \text{ MeV}$), so that the two experi-

ments would complement each other. Although the range we studied is a tiny portion of the phase space, it covers the major part of pion yields, and thus is important for determining average multiplicities of pion production.

The low-energy pions carry unique information on the reaction. The pion absorption cross section in nuclei, empirically deduced by Sparrow *et al.*,⁸ reaches a maximum value at approximately $T_{\pi} \approx 300 \text{ MeV}$ mainly due to the influence of (3, 3) resonance. It decreases monotonically as the pion energy decreases, and below 100 MeV the mean free path of pions in nuclei becomes longer than the size of nuclei. Thus the nuclei are transparent for low-energy pions. Accordingly, we note the following characteristic features:

(1) The low-energy pions produced in a nucleus-nucleus collision ("direct" pions) can easily get out of the system and would carry out direct information on the fast stage of heavy-ion reactions. We, therefore, think that the low-energy pion production probes the more violent aspects of the nucleus-nucleus collisions.

(2) There are, however, other components to the low-energy pion spectra ("secondary" pions) which are generated in secondary processes, such as "moderation" (multiscattering) and "regeneration" (charge exchange) of high-energy pions produced in the reaction.

The low-energy pions we observe should be mixtures of the direct and secondary pions. It would be very helpful in understanding the collision

process if we could find a way to distinguish between the two types of pions experimentally, or empirically, in analyses. Observing the Bose-Einstein effect (Hanbury-Brown-Twiss effect) in two-pion correlations would be a good way to reveal the time-space structure of production of those pions in nucleus-nucleus collisions.⁹ Another reason for this measurement is to understand low-energy pion production, particularly to facilitate extending studies further to include correlation measurements and multiple-pion triggered observations.

II. EXPERIMENTAL

A. Experimental setup

In this work, we studied low-energy pion production in bombardments of the 800-MeV/N ^{20}Ne beam on NaF, Cu, and Pb targets. A layout of the experimental setup is shown in Fig. 1. We used the same target position as Nagamiya and co-workers. The target was located at the center of a rotating table for a magnetic spectrometer, built by Nagamiya *et al.*⁷

The ^{20}Ne beam from the BEVALAC was focused on the target after passing through an ion chamber for beam intensity monitoring and a multiwire ion chamber (MORGADO chamber) for monitoring beam position and size. The ion-chamber reading was recorded for every beam spill. In a series of low-intensity-beam runs, the ion-chamber current was calibrated to counting rates of a plastic scintillation counter inserted into the beam and then extrapolated for use at the higher beam intensities. In order to check the linearity of the ion-chamber response, the calibration was also made with high-intensity beams by measuring ^{11}C radioactivity produced in graphite targets via $^{12}\text{C}(^{20}\text{Ne}, X)^{11}\text{C}$ reactions. The cross section for this reaction was estimated with an accuracy better than 30% from a set of systematic information on the $^{12}\text{C}(p, X)^{11}\text{C}$,¹⁰ $^{12}\text{C}(^{12}\text{C}, ^{11}\text{C})X$,¹¹ and $^{12}\text{C}(^{20}\text{Ne}, X)^{11}\text{C}$ (Ref. 12) reaction cross sections at various energies. The two calibrations agreed within the accuracies of measurements (30%).

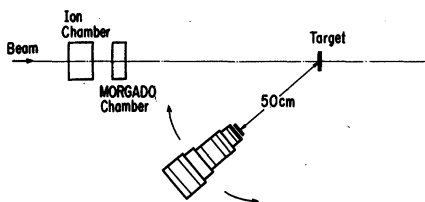


FIG. 1. Schematic diagram of the experimental setup. The target angle to the beam was changed depending on the detector angle.

Signals from the MORGADO chamber were displayed on an oscilloscope monitoring the beam spot throughout the run. The beam spot had to be adjusted only once or twice a day.

Three different targets, NaF, Cu, and Pb, were used to study a mass dependence of the cross sections. The NaF target was chosen because the mass numbers are approximately equal to the projectile ^{20}Ne . Thicknesses of the targets were about 0.5 g/cm^2 in all cases.

We used a pion range telescope which is described in the next subsection. The telescope was mounted on an arm which was rotatable around the target independent of the magnet rotating table. The distance between target and telescope was about 50 cm. The size of a solid-angle-defining scintillator in the telescope was $5 \text{ cm} \times 5 \text{ cm}$, so that the solid angle subtended was about 10 msr. The range of measurement covered by this telescope was $20 \leq T_{\pi}^{\text{Lab}} \leq 100 \text{ MeV}$ and $30^{\circ} \leq \theta^{\text{Lab}} \leq 150^{\circ}$.

Data were taken with a PDP 11/10 via CAMAC and stored in a magnetic tape, event by event. Adjusting the beam intensity, we kept the dead time of the data-taking system at less than 20%. The dead time was measured by counting the "event trigger" signals and the "event accepted" signals [(Event trigger) · (Computer not Busy)].

B. The pion range telescope

For the detection of low-energy pions we developed a pion range telescope. Since a large number of particles of various kinds are emitted in the high-energy heavy-ion reactions, it is very important to use detectors with good particle-identification capabilities. We used the $\pi^+ \rightarrow \mu^+$ decay to identify stopped π^+ 's in the presence of a strong background of other particles (mostly protons). The range telescope used was a stack of plastic scintillators as shown schematically in Fig. 2. When a π^+ enters and stops in one of the scintillators at the position corresponding to the range, the scintillator generates a double pulse, one due to the π^+ , followed by a delayed pulse due to the μ^+ . Since the lifetime of the π^+ is short ($\tau_{\pi} = 26 \text{ nsec}$), for the separation of the delayed μ^+ pulse from the prompt π^+ pulse we made fast clipping of the anode signals of phototubes (RCA 8575 or AMPEREX XP 2230), and we used fast discriminators with good pulse-pair resolutions. The delayed pulse was taken with the fast logic circuit shown schematically in Fig. 2. A difficulty in this method was the fact that the energy of μ^+ is only 4.1 MeV. The energy deposited by the μ^+ should not be too large compared to that of the π^+ . We chose the thickness of the scintillator to be 2.5 or

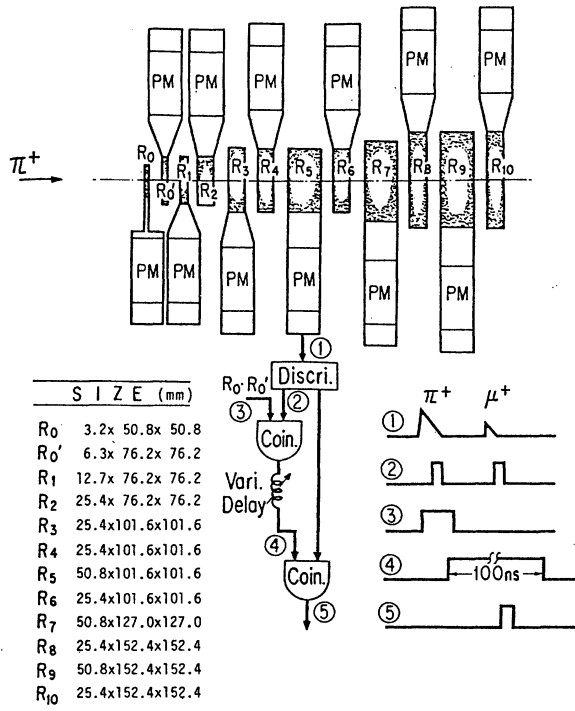


FIG. 2. A schematic diagram of the range telescope, thicknesses, and sizes of the plastic scintillators, and a schematic drawing of the electronic circuit for detecting pion decays.

5.0 cm. The maximum energy deposited by the π^+ in a 2.5-cm plastic scintillator is about 25 MeV. A time spectrum of the delayed pulses was taken for each scintillator. Although it was not possible to avoid a dead region in the time spectra of about 10 nsec, we were able to extrapolate the π^+ decay curve to $t = 0$. Since almost all stopped π^- are captured and disintegrate in a carbon nucleus in the scintillator, instead of decaying into μ^- , this method detects only positive pions.

The concept of range telescopes is not new, but by combining the old method with the current sophisticated CAMAC-computer technique we were able to make the method very powerful. In addition to the delayed-time information, we recorded pulse heights of signals from all scintillators. Thus, by taking the information on the energy deposits in each plastic counter (dE/dx) along the path of a particle, we got a high degree of redundancy in identifying particles or events. For instance, if two protons from different reaction events entered the telescope accidentally with a time difference of a few tens of nsec's, the counter generates a double pulse. This accidental event was a serious source of the constant background in time spectra, particularly when the telescope was set at forward angles where more

than 100 times more protons than pions passed through the telescope. However, these "background" events were easily cleaned up by use of the pulse-height information. We will discuss more technical details of the instrumentation in a separate publication.

III. RESULTS

Doubly differential cross sections for the low-energy positive pion production obtained are listed in Table I and plotted in Fig. 3. The errors shown are only statistical ones for individual

TABLE I. Cross section for π^+ from NaF, Cu, and Pb in $\mu\text{b}/\text{sr MeV}$. (Numbers in parentheses are uncertainties.)

Pion energy T_{π}^{Lab} (MeV)	Angle $\theta_{\pi}^{\text{Lab}}$ (Degrees)					
	30	45	58	90	120	150
NaF						
19	113 (10)	87 (6)	79 (6)	87 (6)	134 (6)	125 (7)
29	113 (10)	124 (8)	98 (7)	113 (6)	152 (6)	136 (6)
40	165 (13)	151 (9)	127 (7)	137 (6)	165 (6)	151 (6)
49	189 (15)	193 (10)	138 (8)	145 (7)	169 (6)	146 (6)
61	...	189 (10)	166 (8)	137 (6)	158 (5)	114 (6)
72	186 (18)	207 (11)	158 (9)	115 (6)	123 (7)	90 (7)
83	212 (18)	220 (13)	154 (11)	110 (9)	102 (7)	75 (5)
93	190 (18)	211 (13)	152 (10)	90 (8)	79 (5)	45 (5)
102	228 (24)	218 (16)	128 (12)	76 (10)	56 (7)	26 (8)
Cu						
19	202 (29)	188 (19)	194 (16)	196 (9)	259 (13)	208 (20)
29	235 (23)	208 (20)	220 (17)	256 (10)	327 (13)	261 (16)
40	255 (31)	264 (22)	314 (19)	317 (12)	358 (13)	281 (18)
49	333 (36)	318 (24)	350 (20)	327 (12)	356 (14)	275 (18)
61	...	390 (22)	371 (16)	301 (10)	260 (15)	233 (16)
72	309 (45)	314 (26)	364 (20)	249 (17)	239 (16)	157 (16)
83	309 (39)	356 (32)	349 (28)	232 (18)	224 (12)	103 (15)
93	231 (40)	361 (30)	313 (22)	189 (13)	151 (13)	100 (14)
102	246 (55)	295 (33)	300 (28)	177 (17)	132 (13)	56 (9)

TABLE I. (Continued).

Pion energy T_{π}^{Lab} (MeV)	Angle $\theta_{\pi}^{\text{Lab}}$ (Degrees)					
	30	45	58	90	120	150
Pb						
19	310 (62)	386 (40)	279 (36)	248 (25)	391 (29)	412 (27)
29	340 (42)	401 (35)	333 (26)	310 (20)	567 (23)	532 (25)
40	616 (62)	447 (53)	442 (28)	468 (24)	621 (28)	617 (37)
49	656 (67)	592 (48)	503 (37)	474 (27)	674 (26)	602 (29)
61	...	623 (42)	513 (35)	450 (24)	624 (24)	534 (25)
72	631 (79)	570 (56)	508 (40)	413 (34)	477 (34)	417 (29)
83	602 (81)	686 (60)	531 (37)	417 (20)	403 (32)	316 (25)
93	613 (75)	502 (58)	397 (38)	287 (28)	323 (26)	216 (20)
102	606 (95)	569 (69)	448 (47)	231 (32)	229 (27)	178 (22)

numbers. Other sources of errors were uncertainties from the beam-intensity calibration and from various corrections for detection of pions, and ambiguities in subtracting background owing to the beam halo hitting materials around the target. The overall uncertainties for the absolute values of the cross sections were about 30%.

For the reduction of raw data to final cross sections, the following facts were carefully

checked, and necessary corrections were made:

(1) *Decay in flight*. The probability of the pion decay in flight was calculated for the actual geometrical arrangement. The correction factors for all scintillation counters were almost the same (~15%).

(2) *Nuclear reaction*. Corrections were made for the loss of pions due to nuclear reactions with nuclei in the plastic scintillator (mostly the ^{12}C). This correction, however, was the largest source of uncertainties because no good cross section data for the $\pi^+ + ^{12}\text{C}$ reaction are available for the low-energy region. We calculated the correction factor due to nuclear reactions using the empirical formula¹³ of the pion-nucleus cross sections, similar to the method used in Ref. 14. It was checked also by means of an optical-model calculation.¹⁵ Results of these two different methods were in good agreement. The typical correction factors were 10% for 60-MeV pions and 30% for 100-MeV pions.

(3) *Multiple scattering and edge effects*. The corrections for pions escaping from the range telescope due to multiple Coulomb scattering were calculated with the empirical formula for the deflection angle via multiple Coulomb scattering.¹⁶ Since the telescope was designed to make the size of each element gradually larger from the front to the back, the correction factors were small (<5%).

When a pion stopped near the edge of a scintillator and the muon escaped from the counter

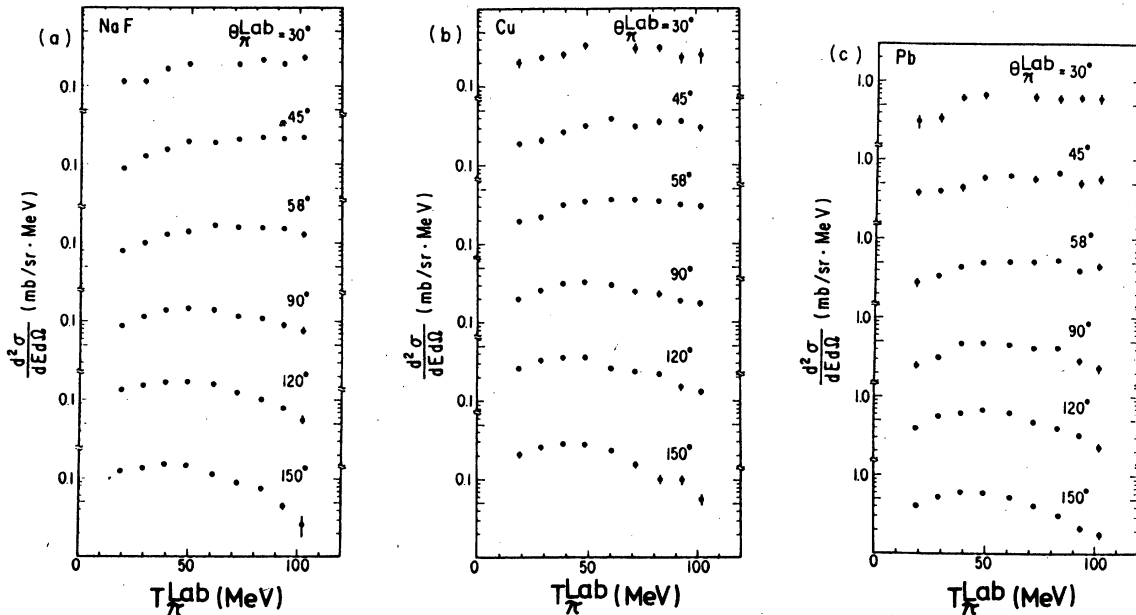


FIG. 3. Doubly differential cross sections for positive pion production with the 800 MeV/N ^{20}Ne beam on (a) NaF, (b) Cu, and (c) Pb targets, respectively. The errors are only statistical ones.

TABLE II. Energy acceptance and mean energy of pion stopped in each element of the telescope (in units of MeV). These values depend on the target thickness and angle to the detector direction. Here, three typical examples are listed: in column (a) without taking into account the target thickness, (b) with the NaF target at a 60° angle to the detector, and (c) with the Pb target at the same angle.

Element	(a)		(b)		(c)	
	Mean energy	Energy acceptance	Mean energy	Energy acceptance	Mean energy	Energy acceptance
R_1	18.5	8.1	19.7	7.8	19.3	7.9
R_2	28.5	12.0	29.4	11.8	29.2	11.8
R_3	39.4	9.8	40.2	9.7	40.0	9.7
R_4	48.7	8.7	49.3	8.6	49.1	8.6
R_5	60.8	15.5	61.4	15.5	61.2	15.5
R_6	72.1	7.2	72.6	7.2	72.5	7.2
R_7	82.5	13.6	83.0	13.5	82.9	13.6
R_8	92.5	6.5	93.0	6.5	92.9	6.5
R_9	102.0	12.6	102.5	12.6	102.4	12.6

without depositing energy above the discriminator threshold, no triggering occurred. This effect was again small (<5%). However, we made corrections for both effects.

(4) *Thickness of the target and scintillators.* The measurement with the telescope was for counting pions in a certain interval of energy which was determined by the thicknesses of the scintillators and the target. The energy acceptance (ΔE) and central energy for each scintillator were calculated using an empirical formula for the stopping power (dE/dx) in the plastic and the targets. Those values depend slightly on the target thickness and angle to the direction of the detector. Typical examples are shown in Table II.

(5) *Background.* In order to subtract background pions we took the data always with and without the target. The background pions observed in the run without the target were considered to be mainly those from the target frame, tag counters, etc. hit by the beam halo.

IV. DISCUSSION

A. Pions from the NaF target

Since the mass numbers of Na and F are approximately equal to that of the projectile ^{20}Ne , transformation of the experimental cross sections in the laboratory (Lab) frame to the center-of-mass (c.m.) frame is straightforward. Figure 4(a)

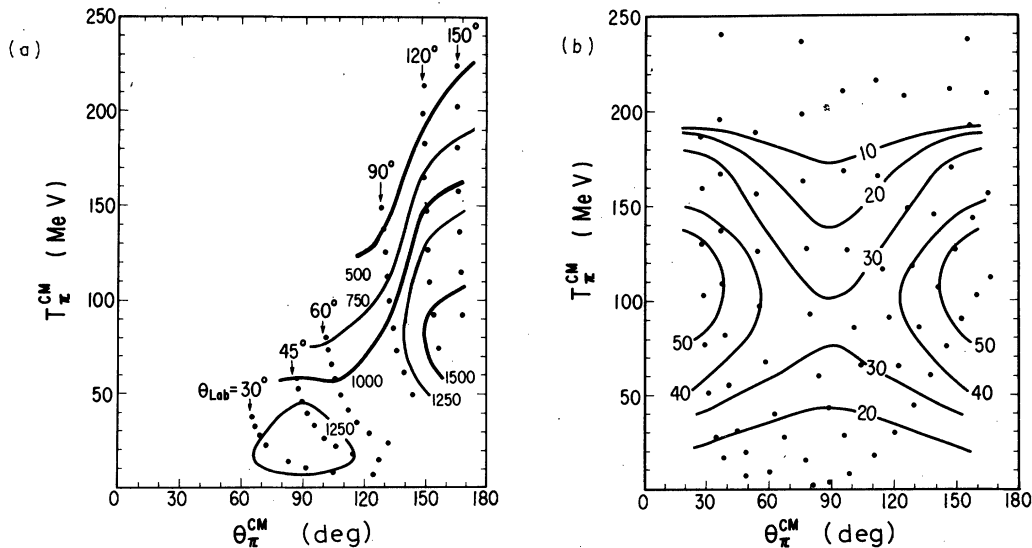


FIG. 4. Contour plots of the Lorentz-invariant cross sections (a) for $^{20}\text{Ne} + \text{NaF} \rightarrow \pi^+ + \text{anything}$ at 800 MeV/N, and (b) for $p + p \rightarrow \pi^+ + \text{anything}$ at 730 MeV (Ref. 17). The numbers written along with the contour lines are invariant cross sections in units of $\text{mb sr}^{-1}(\text{GeV})^{-1}c$. The black dots indicate the observed points. The contour lines should be symmetric about $\theta_{\pi}^{\text{c.m.}} = 90^\circ$.

shows a contour of the Lorentz-invariant cross sections $(1/p)(d^2\sigma/dEd\Omega)$ in a plane of $T_\pi^{\text{c.m.}}$, the kinetic energy of pions in the c.m. frame, and $\theta_\pi^{\text{c.m.}}$, the c.m. angle. Although our data do not cover the whole range of $\theta_\pi^{\text{c.m.}}$, the plot must be symmetric about $\theta_\pi^{\text{c.m.}} = 90^\circ$, permitting us to reflect data points about 90° c.m. as a check.

For comparison with the free nucleon-nucleon process, the same plot for the $(p+p \rightarrow \pi^+ + \text{anything})$ process at 730 MeV is shown in Fig. 4(b). The plot was made with the data by Cochran *et al.*¹⁷ For a strict comparison, we would have to include pions from the $(p+n \rightarrow \pi^+ + \text{anything})$, but its contribution is small [$\sim 20\%$: $\sigma(p+n \rightarrow \pi^+ + X) = 3$ mb, $\sigma(p+p \rightarrow \pi^+ + X) = 16$ mb for $E = 800$ MeV], and we do not make the comparison to that accuracy.

Comparing Figs. 4(a) and 4(b), we observe the following points:

- (1) The angular and energy distribution of π^+ from the $^{20}\text{Ne} + \text{NaF}$ process is significantly different from the free nucleon-nucleon process.
- (2) The intermediate-energy region ($50 \leq T_\pi \leq 250$ MeV) of the distribution, however, apparently shows a marked similarity to the free nucleon process. The characteristic peak of the nucleon-nucleon collision at 180° and around 100 MeV in the center-of-mass system appears to remain.
- (3) While the angular distribution is forward and backward peaked at higher energies ($T_\pi \geq 50$ MeV), at lower energies it is more isotropic and shows a broad peak at 90° .

These facts seem to indicate that most of the intermediate-energy pions come from individual nucleon-nucleon collisions modified by Fermi motion. Clearly, there must be secondary processes, such as thermalization or rescattering effects, to account for the low-energy part of the distribution. The broad peak at 90° in the low-energy region (around 30 MeV) is very interesting. Wolf *et al.*¹⁸ have recently reported similar observations of a low-energy 90° (c.m.) π^+ peak in $^{20}\text{Ne} + ^{27}\text{Al}$ and $^{40}\text{Ar} + ^{40}\text{Ca}$ systems at 1.0 GeV/N.

B. Comparison with a superposition of the $(p + \text{nucleus})$ cross section

In order to search for effects in the pion production specific to the heavy-ion reaction, we compared our heavy-ion data with an incoherent superposition of the cross sections for the reactions, proton + nucleus $\rightarrow \pi^+ + X$.

We made the simple estimate from the $(p + \text{nucleus})$ cross sections using the data by Cochran *et al.*,¹⁷ who measured the pion-produc-

tion cross section with 730-MeV protons on various targets (H, D, Be, C, Al, Ti, Cu, Ag, Ta, Pb, and Th). They observed pions with energies from 30 to 550 MeV at angles between 15° and 150° .

Assuming no coherence among nucleons in the projectile ^{20}Ne , we calculated the cross section with the formula

$$\begin{aligned} \left(\frac{d^2\sigma}{dEd\Omega}\right)_{\text{Proj} + T - \pi^+ + X} &= Z_{\text{Proj}} \left(\frac{d^2\sigma}{dEd\Omega}\right)_{p + T - \pi^+ + X} \\ &+ N_{\text{Proj}} \left(\frac{d^2\sigma}{dEd\Omega}\right)_{n + T - \pi^+ + X} \\ &= Z_{\text{Proj}} \left(\frac{d^2\sigma}{dEd\Omega}\right)_{p + T - \pi^+ + X} \\ &+ \left(\frac{Z}{N}\right)_T N_{\text{Proj}} \left(\frac{d^2\sigma}{dEd\Omega}\right)_{p + T - \pi^- + X}, \end{aligned}$$

where $Z_{\text{Proj}} = 10$, $N_{\text{Proj}} = 10$, and T stands for the target. Because there are no data on pion-production cross sections from neutron bombardment in this energy region, the second term was replaced by the π^- production cross section from protons, assuming charge symmetry. Moreover, the factor $(Z/N)_T$ has to be multiplied to take into account the fact that the proton and neutron numbers in the target are different. This replacement is only an approximation, but we note that the contribution of the second term is much smaller than that of the first term, so that the ambiguity of the approximation does not affect the summed results so much.

Figure 5 shows a comparison between the calculated cross sections and the experimental data in the case of the Pb target. Despite the approximate nature of the expressions, the agreement between calculation and experiment is rather good. In this calculation the effects of pion absorption, scattering, and charge exchange in the target nucleus are included automatically by using the experimental data. Such effects in the projectile nucleus, however, are not taken into account by this calculation. Although the Fermi motion of nucleons in the projectile and the difference of the incident energies between 730 and 800 MeV/N were ignored, these effects should not be large, because the dependence on the incident energy of the pion-production cross section in the nucleon-nucleon collision at this energy is weak. We extended the calculation to higher-energy pions to compare with the data by Nagamiya *et al.*¹⁹ As shown in Fig. 6, agreement between the calculation and the experiment is very good up to 0.5 GeV/c. The data do seem to show a tail extending to higher energies than our calculation, presum-

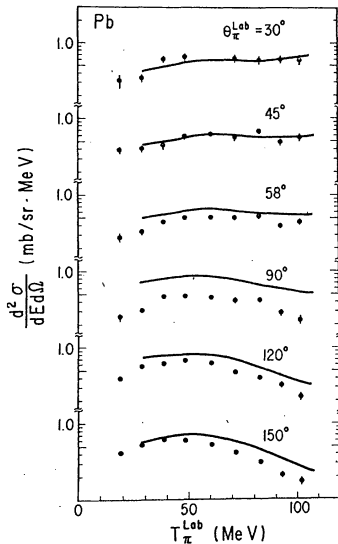


FIG. 5. Comparison of the experimental cross section (black dots) for $^{20}\text{Ne} + \text{Pb} \rightarrow \pi^+ + \text{anything}$ with the calculation based on the incoherent superposition of the cross sections for $p + \text{Pb} \rightarrow \pi^+ + \text{anything}$.

ably a reflection of there being neglected Fermi motion in the projectile.

V. SUMMARY

The observed angular distribution of low-energy pions in the nucleon-nucleon center of mass ($T_{\pi}^{\text{c.m.}} \leq 50$ MeV) is essentially isotropic with some peaking at 90° , while the intermediate-energy part ($50 \leq T_{\pi}^{\text{c.m.}} \leq 300$ MeV) is forward and backward peaked. It has been shown by Nagamiya *et al.*⁷ that in the higher-energy region ($T_{\pi}^{\text{c.m.}} \leq 400$ MeV) the distribution approaches isotropy.

The intermediate-energy part of the distributions appears to reflect the individual nucleon-nucleon process, and those pions are considered to be emitted from the decay of the (3, 3) resonances produced. On the other hand, the major part of the low-energy pions are considered to be the "secondary" pions. In particular, those in the region around $\theta_{\pi}^{\text{c.m.}} = 90^\circ$ [Fig. 4(a)] are mostly from the central region, while around $\theta_{\pi}^{\text{c.m.}} = 0^\circ$ or 180° there must be contributions of pions from projectiles or target fragments. The broad bump at 90° will be more pronounced if we subtract

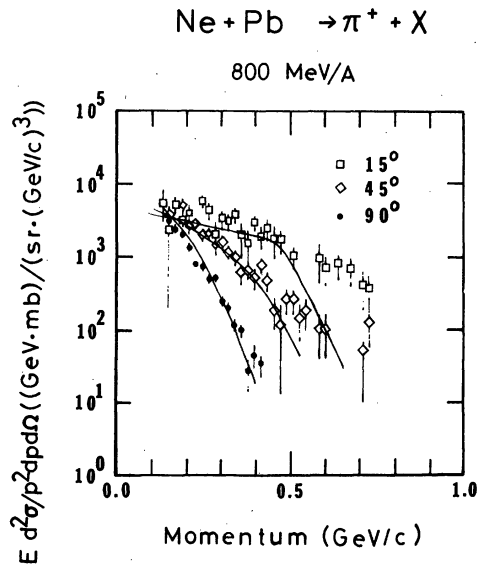


FIG. 6. Comparison of the calculated cross sections with experimental results by Nagamiya *et al.* (Ref. 19) for higher-energy pions.

those contributions. It would be very interesting to study further the origin of those excess pions in their dependence on bombarding energy and target and projectile mass. The good agreement of the incoherent superposition of (proton + nucleus) cross sections with experiments indicates the individual nucleon-nucleon collision nature of the process for most of the pion production.

ACKNOWLEDGMENTS

We are very grateful to the BEVALAC staff and operators for their excellent support of the experiments. We are indebted to the technical staff at Lawrence Berkeley Laboratory: G. Constantian for electronics, J. Harvill for computer hardware, and many other people. Thanks are also due to Dr. M. Sasao, Miss M. Sekimoto, and Dr. R. S. Hayano for their help at various stages of the experiments. This work was supported by the Nuclear Science Division of the U.S. Department of Energy under Contract No. W-7405-ENG-48, and by the Mitsubishi Foundation (Japan) and the Japan Society for the Promotion of Science, and had the endorsement of the National Science Foundation.

¹A. M. Baldin, S. B. Garasimov, H. Guordenescu, V. N. Zubarev, L. K. Ivanova, A. D. Kirillov, V. A. Kuznetsov, N. S. Moroz, V. B. Radomanov, V. N. Ramzhin, V. S. Stavinskii, and M. I. Ytsuta, *Yad. Fiz.* **18**, 79 (1974) [*Sov. J. Nucl. Phys.* **18**, 41 (1974)].

²W. Schimmerling, K. G. Vosburgh, K. Koepke, and W. D. Wales, *Phys. Rev. Lett.* **33**, 1170 (1974).

³J. Papp, J. Jaros, L. Schroeder, J. Staples, H. Steiner, A. Wagner, and J. Wiss, *Phys. Rev. Lett.* **34**, 601 (1975); J. Papp, Ph.D. thesis, LBL Report No. 3633,

- (1975).
- ⁴B. Jakobsson, R. Kullberg, I. Otterlund, A. Ruiz, J. M. Bolta, and E. Higon, Contribution to the VIIth International Conference on High-Energy Physics and Nuclear Structure, Zurich, 1977 (unpublished).
- ⁵S. Y. Fung, W. Gorn, G. P. Kiernan, F. F. Liu, J. J. Lu, Y. T. Oh, J. Ozawa, R. T. Poe, L. Schroeder, and H. Steiner, *Phys. Rev. Lett.* **40**, 292 (1978).
- ⁶M. Gyulassy and S. K. Kauffmann, *Phys. Rev. Lett.* **40**, 298 (1978).
- ⁷S. Nagamiya, I. Tanihata, S. Schnetzer, L. Anderson, W. Bruckner, O. Chamberlain, G. Shapiro, and H. Steiner, in *Proceedings of the International Conference on Nuclear Structure, Tokyo, 1977*, edited by T. Marumori (Physical Society of Japan, Tokyo, 1978); *J. Phys. Soc. Japan* **44**, Suppl. 378 (1978).
- ⁸D. A. Sparrow, M. M. Sternheim, and R. R. Silbar, *Phys. Rev. C* **10**, 2215 (1974).
- ⁹G. I. Kopylov and M. I. Podgoretskii, *Yad. Fiz.* **15**, 392 (1972) [*Sov. J. Nucl. Phys.* **15**, 219 (1972)]; **19**, 434 (1974) [**19**, 215 (1974)]; G. Cocconi, *Phys. Lett.* **49B**, 459 (1974).
- ¹⁰J. B. Cumming, *Annu. Rev. Nucl. Sci.* **13**, 260 (1963).
- ¹¹D. E. Greiner, P. J. Lindstrom, H. H. Heckman, Bruce Cork, and F. S. Beiser, *Phys. Rev. Lett.* **35**, 152 (1975).
- ¹²A. R. Smith and R. H. Thomas, LBL Report No. 3861, 1975.
- ¹³C. Richard-Serre and M. J. M. Saltmarsh, *Nucl. Instrum. Methods* **63**, 173 (1968).
- ¹⁴P. W. James, D. A. Bryman, G. R. Mason, L. P. Robertson, T. R. Witten, and J. S. Vincent, TRIUMF Report No. TRI-PP-76-3, 1976.
- ¹⁵M. Sasao, private communication.
- ¹⁶Particle Properties Booklet, CERN, 1976, p. 72.
- ¹⁷D. R. F. Cochran, P. N. Dean, P. A. M. Gram, E. A. Knapp, E. R. Martin, D. E. Nagle, P. B. Perkins, W. J. Shlaer, H. A. Thiessen, and E. D. Theriot, *Phys. Rev. D* **6**, 3085 (1972).
- ¹⁸K. L. Wolf *et al.*, *Bull. Am. Phys. Soc.* **23**, 959 (1978), Abstract FB 10.
- ¹⁹S. Nagamiya *et al.*, unpublished data.